



ORIGINAL ARTICLE

Facile synthesis of ZnO/CuO/Eu heterostructure photocatalyst for the degradation of industrial effluent



J.P. Shubha^{a,*}, B. Roopashree^b, R.C. Patil^c, Mujeeb Khan^d,
Mohammed Rafi Shaik^d, Marwa Alaqarbeh^e, Abdulrahman Alwarthan^d,
Abdulnasser Mahmoud Karami^d, Syed Farooq Adil^{d,*}

^a Department of Chemistry, Sri Jaychamarajendra College of Engineering, JSS Science & Technology University, Mysuru 570006, India

^b Department of Chemistry, JSS Academy of Technical Education, Dr. Vishnuvardhan Road, Bangalore 560060, India

^c Department of Electronics and Communication Engineering, Jain College of Engineering, Machhe, Belagavi 590014, India

^d Department of Chemistry, College of Science, King Saud University, P.O. Box 2455, Riyadh 11451, Saudi Arabia

^e National Agricultural Research Center, Al-Baq'a 19381, Jordan

Received 6 November 2022; accepted 3 January 2023

Available online 6 January 2023

KEYWORDS

Ternary heterostructure;
ZnO/CuO/Eu;
Photocatalyst;
Methylene blue;
Rhodamine-B;
UV irradiation, dye degradation;
Industrial effluent

Abstract Zinc oxide-based ternary heterostructure ZnO/CuO/Eu(1%, 3%, and 5% of Eu) nanoparticles were effectively produced by employing *Vigna unguiculata* (cowpea) waste skin extract as fuel in a simple one-pot combustion process. The as-synthesized heterostructure was analyzed by X-ray diffraction studies, ultraviolet-visible spectroscopy, Fourier Transform Infrared Spectroscopy, Field Emission Scanning Electron Microscopy, and High-Resolution Transmission Electron Microscopy techniques. Besides, the photocatalytic degradation efficiency of the as-obtained ternary nanocomposite was evaluated under UV light for the degradation of model organic pollutants including methylene blue (MB), Rhodamine-B (RB), and an effluent sample collected from the textile industrial waste. During this study, the effect of a variety of parameters on the photodegradation activity of the photocatalysts has been thoroughly evaluated, such as light source, catalyst dose, irradiation period, dye concentration, solution pH, etc. Under UV irradiation (100 mins), the ternary ZnO/CuO/Eu photocatalyst demonstrated excellent degradation activity of ~99 and ~93% for MB and RB, respectively, while for the industrial effluent, a decent degradation activity of 42% has been recorded. Further experiments have revealed a pH and concentration-dependent

* Corresponding authors.

E-mail addresses: shubhapranesh@gmail.com (J.P. Shubha), sfadil@ksu.edu.sa (S.F. Adil).

Peer review under responsibility of King Saud University.



photocatalytic behavior of the heterostructure photocatalyst. Therefore, the results suggest that the heterostructure photocatalyst can be potentially applied for wastewater treatment and other environmental applications.

© 2023 Published by Elsevier B.V. on behalf of King Saud University. This is an open access article under the CC BY-NC-ND license (<http://creativecommons.org/licenses/by-nc-nd/4.0/>).

1. Introduction

Semiconductor-based photocatalytic degradation of hazardous dyes offers great potential in addressing the fast-growing issue of environmental pollution (Natarajan et al., 2018). Particularly, the toxic organic dyes used in the textile industry are specifically regarded as a serious environmental threat, due to their inherent color and capacity to absorb dissolved oxygen from water bodies (Bharagava and Chowdhary, 2019). These types of hazardous organic dyes can potentially disrupt the natural photosynthetic process by inhibiting the ability of sunlight to penetrate water bodies, which ultimately has a significant impact on the aquatic environment (Pereira and Alves, 2012). Additionally, due to their high stability, these organic pollutants can exist in the environment for a longer period, and thus are considered xenobiotics (Khan and Malik, 2014; Malik et al., 2014). Therefore, untreated textile effluent poses a great risk to both terrestrial and aquatic life by degrading the natural ecosystem and having a severe impact on long-term health (Rovira and Domingo, 2019). As a result, numerous physicochemical and biological mechanisms have been used to degrade organic dyes, and other new techniques are currently being actively investigated (Chiu et al., 2019; Dai et al., 2022; Hannachi and Hafidh, 2020; Paiman et al., 2020; Pandey et al., 2015; Paździor et al., 2019; Wu et al., 2020). The cost-effective removal of these colours from effluents is still a significant issue (Dai et al., 2021; Lv et al., 2019).

Recently, the application of sophisticated oxidation techniques has attracted a lot of scientific interest in the degradation of hazardous dyes from industrial effluents (Hassaan et al., 2017; Wang et al., 2022). These procedures possess a strong ability to degrade a variety of complex dyes and hazardous organic compounds from wastewater and have also been proven to be economical and environmentally friendly (Mehrizad and Gharbani, 2014; Tabatabaei et al., 2011). Advanced oxidation processes are often carried out under light irradiation including solar or ultraviolet light in the presence of photocatalysts (Ataei et al., 2021; Qrajhdaghy et al., 2022). While, in several cases, H_2O_2 and ultrasonication have also been utilized to accelerate the process of adsorption or degradation of dyes on the surface of photocatalysts (Navarro et al., 2017). Among a variety of catalysts, semiconductor-based photocatalysts like Fe_2O_3 , CdS, V_2O_5 , ZnO, ZrO_2 , TiO_2 , and others have been widely used for the degradation of hazardous organic dyes (Belver et al., 2019; Mehrizad and Gharbani, 2017; Mosavi et al., 2021; Shaik et al., 2020). Particularly, ZnO-based photocatalysts have been widely used in the field of environmental remediation due to their high chemical stability, excellent biocompatibility, distinctive electrical structure, and lower price (Lavand and Malghe, 2015; Pirhashemi et al., 2018; Wetchakun et al., 2019).

However, the practical applications of ZnO have been mostly hindered by the large band gap and quick recombination of photoinduced charge carriers. Therefore, ZnO is frequently modified by structural doping with both metallic and non-metallic materials. Besides, the techniques of fabricating heterojunctions with a second semiconductor component have also been widely used to improve charge separation and enhance the sensitivity of ZnO toward the visible light (Zeelani et al., 2016). Indeed, the later process of creating heterojunctions offers exciting probabilities of improving the separation effectiveness of photoinduced charge carriers (Kumar et al., 2020). Due to this, so far, numerous ZnO-based binary and ternary heterojunctions, including 2D ZnO/ZnS binary heterostructures, ternary heterostructures of

ZnO/Cu₂O/Si nanowire arrays, and ZnOZnSGd₂S₃ nanostructural arrays, have been successfully fabricated (Hsiao et al., 2019; Ranjith et al., 2020; Wei et al., 2019; Yu et al., 2019).

Therefore, multicomponent photocatalysts based on rationally designed ZnO-based ternary heterojunctions, which typically facilitate electron migration, offer considerable potential for the photocatalytic degradation of organic dyes (Wang et al., 2019). These devices efficiently increase the range of light absorption and prolong the lifetime of photogenerated charge carriers (Kumar et al., 2020). However, the fabrication of effective and affordable multicomponent heterojunctions is still challenging, due to the high-cost, low-stability, less environmental compatibility of commonly applied precursors. These kinds of systems are typically created using a variety of physical and chemical techniques, such as sol-gel, chemical vapor deposition, microwave heating, coprecipitation, and hydrothermal and solvothermal techniques (Lee et al., 2016). These approaches often require expensive equipment, prolonged reaction times, and higher temperatures; as a result, the development of more simple procedures is highly crucial.

Solution combustion, on the other hand, is a simple approach that is inexpensive, time and energy efficient, and easy to use, which can also be scaled up to obtain large quantities of nanomaterials (Kumar et al., 2017). Combustion processes are self-propagating high-temperature methods involving an external thermal source which ignites exothermic reaction mixture (Varma et al., 2016). This causes a rapid increase in the temperature (1000–3000 °C) which propagates through the heterogeneous mixture in a self-sustained manner leading to the formation of the solid material (Aruna and Mukasyan, 2008). Typically, the initial reaction medium in conventional combustion synthesis is a powder mixture, however, when it is replaced with reactive solution, the process is referred as solution combustion (Wen and Wu, 2014). This method usually involves a self-sustained reaction in solutions of metal nitrites and different fuels. In other words, liquid solutions of desired reagents, when heated to a moderate temperature (150–200 °C), ignite themselves leading to a rapid increase in the temperature, which ultimately facilitate the formation of fine solid products with tailored composition (Xu et al., 2019). This technique has been effectively utilized for the preparation of a variety of advance nanomaterials using different types of fuels and raw materials (Siddique et al., 2022).

Additionally, this process can also be successfully used with eco-friendly raw materials as reported in our previous studies (Adil et al., 2013; Aruna and Mukasyan, 2008; Saif et al., 2019). Therefore, herein we have investigated the production of ZnO-based ternary heterojunctions involving other components like photoactive metal oxide (CuO) and a lanthanide (Eu) using a facile solution combustion process. The as-prepared heterostructure nanomaterial was further used as a photocatalyst for the degradation of methylene blue (MB), Rhodamine-B (RB) and effluent collected from textile industry under UV irradiation.

2. Materials and methods

With no further purification, raw materials of analytical grades such as zinc nitrate hexahydrate ($Zn(NO_3)_2 \cdot 6H_2O$ (Sigma-Aldrich)), copper acetate monohydrate ($Cu(CH_3CO_2)_2 \cdot H_2O$ (Sigma-Aldrich)) and europium nitrate hydrate ($Eu(NO_3)_3 \cdot 5H_2O$ (Sigma-Aldrich)) are employed. To make a model waste

water sample containing methylene blue (SD fine chemicals) and Rhodamine -B (SD fine chemicals) dye solutions are prepared with distilled water. Effluent collected from nearby dyeing unit is filtered, centrifuged and used.

2.1. Synthesis of ZnO/CuO/Eu

In 10 mL of distilled water, stoichiometrically calculated amounts of zinc nitrate, copper acetate, and europium nitrate 48.5 wt% $\text{Zn}(\text{NO}_3)_2$, 48.5 wt% $\text{Cu}(\text{CH}_3\text{CO}_2)_2$, and 3 wt% $\text{Eu}(\text{NO}_3)_3 \cdot 5\text{H}_2\text{O}$ are dissolved, and 4.5 mL of cowpea (*Vigna unguiculata*) skin extract is added. The mixture is then continuously stirred for 20 min on hot plate maintained at 60 °C. The thoroughly mixed reaction mixture is then inserted into a muffle furnace which is adjusted and maintained at 400 °C. A dark brownish powder is produced after 10 min, which is calcined at the same temperature for 3 h. Cowpea extract was prepared by boiling 50 g of cowpea skin in 200 mL of distilled water for 50 min. Then the filtrate was used for the synthesis of ZnO/CuO/Eu NPs.

3. Results and discussion

3.1. UV–Vis spectrum

The UV–vis absorption spectrum of the as-prepared ZnO/CuO/Eu NPs is displayed in Fig. 1(A). The as-prepared heterostructure reveals absorption bands throughout the spectrum, however as previously reported by Khorsand Zak et al. the band gap calculations are carried out by initially evaluating the first derivative of the absorbance spectrum and finding the maximum in the derivative spectrum in the sides of lower energy (Zak et al., 2011). The band gap calculated was 3.3 eV Fig. 1(B). A wide range of absorption of light helps in effective photocatalytic degradation and enhances the efficiency (Shubha et al., 2021).

3.2. X-ray diffraction

The prepared mixed metal oxides are subjected to X-ray diffraction (XRD), and the obtained diffractograms are shown in Fig. 2. A comparative XRD of CuO, ZnO, and Eu are also

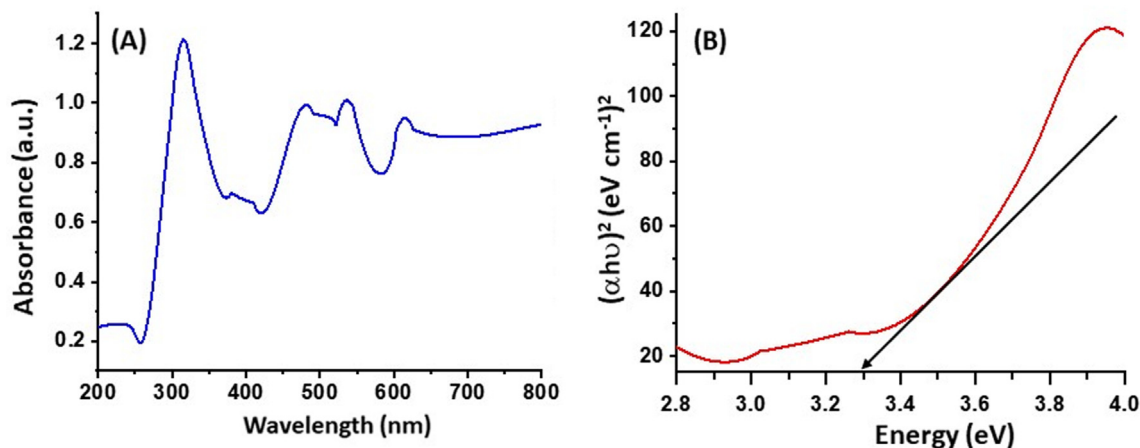


Fig. 1 (A) UV–Visible spectrum and (B) band gap spectrum of as prepared ZnO/CuO/Eu heterostructure.

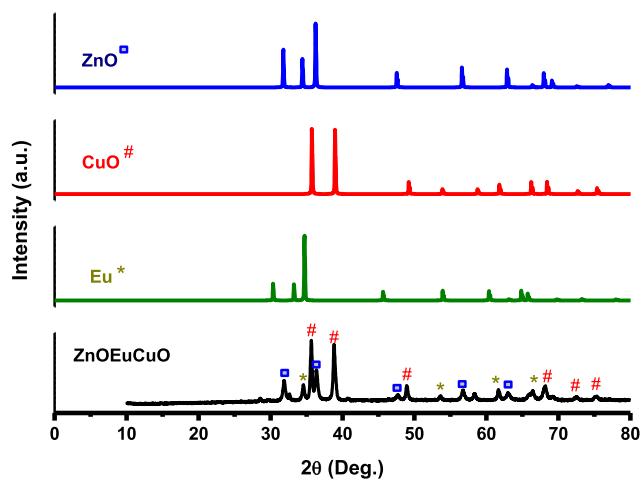


Fig. 2 XRD patterns of ZnO/CuO/Eu nanostructure and a comparative ZnO, CuO and Eu diffraction patterns.

included in this figure. The evaluation of the diffraction pattern obtained for ZnO/CuO/Eu NPs provides evidence that the as-prepared heterostructures are crystalline in nature. The pattern obtained corresponds to the mixture comprising hexagonal structures of ZnO, CuO, and Eu. The powder diffraction pattern of CuO is shown with monoclinic structures (JCPDS no: 1-1117) with a lattice parameter $a = 4.653 \text{ \AA}$, $b = 3.410 \text{ \AA}$, $c = 5.108 \text{ \AA}$ and with a space group C2/c (no. 15). Hexagonal Eu NPs are shown with a heterostructure (JCPDS no 65-368), a lattice parameter $a = 3.39800$, $c = 5.38500$ and a space group P63/mmc (no. 194). Moreover, Fig. 2 also shows that the diffraction pattern obtained for ZnO is similar to the reference XRD pattern of ZnO obtained from ICSD, which is hexagonal with the heterostructure (JCPDS no 36-1451) and lattice parameters $a = 3.24982 \text{ \AA}$ and $c = 5.20661 \text{ \AA}$, while the space group is P63mc (no. 186).

3.3. FT-IR spectrum

Fig. 3 shows the ZnO/CuO/Eu NPs' FTIR spectrum. A CuO NP's FTIR spectrum displays large absorption bands between 2800 and 4000 cm^{-1} , which are primarily attributed to OH from the hydroxyl group and are likely caused by water that

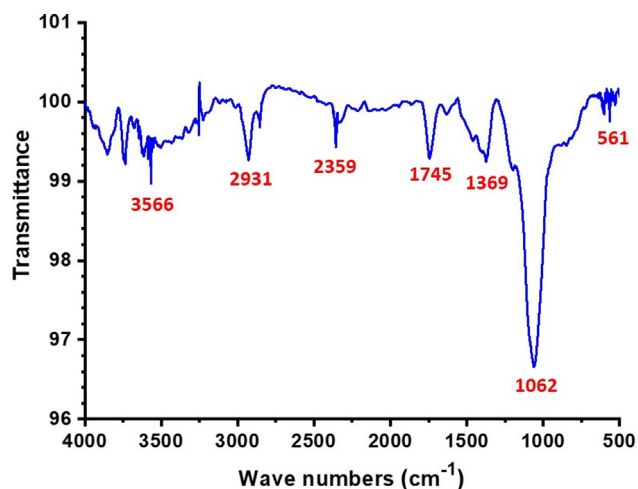


Fig. 3 FTIR spectrum of as-prepared ZnO/CuO/Eu heterostructure.

has been adsorbed from the atmosphere on the NPs' surfaces as well as C-O (due to atmospheric carbon dioxide) groups on the surfaces of ZnO/CuO/Eu NPs (Padil and Černík, 2013). The development of the Eu phase is characterized by a peak at 3566 cm^{-1} (Mohamed and Abu-Dief, 2018). The C=O stretching of acetate causes a peak to appear at 1062 cm^{-1} . The M-O and M-O-M stretching modes of vibrational frequencies of metals interconnected by common oxygen atoms, which are also visible in the FTIR spectrum of ZnO, are responsible for the characteristic peaks less than 1000 cm^{-1} , i.e. 561 cm^{-1} (Julien and Nazri, 1998).

3.4. Microscopic analysis

3.4.1. SEM analysis

The morphological features of the as-prepared heterostructure, that is, ZnO/CuO/Eu, are obtained by field emission scanning electron microscopy (FESEM) analysis, and the achievement of the nanostructured heterostructure is confirmed by TEM analysis, and the results obtained are given in Figs. 4 and 5.

The low-magnification FESEM image shown in Fig. 4a reveals that ZnO/CuO/Eu is composed of clusters of particles as well as flakes. Fig. 4b is the high-magnification FESEM image which shows that part of the material is in the form of flakes in which all the flakes are interconnected and form a net-like structure with large pores. Based on the previously reported literature, it can be assumed that the flake-like morphology could belong to the CuO component of the heterostructure, while the clusters could be the ZnO and Eu NPs in the heterostructure (Ma et al., 2019).

3.4.2. TEM analysis

Fig. 5 shows the TEM images of the ZnO/CuO/Eu heterostructure. Fig. 5a–c shows the low- and high-magnification images which demonstrate that the spherical particles are distributed all over the sample, as well as some incidents of agglomerations, can be observed. The sizes of the particles are in the range between 20 and 60 nm. The selected area electron diffraction pattern (Fig. 5d) indicates a polycrystalline form of the material, and the reflection planes obtained are very much in alignment with the information deduced from the XRD pattern.

3.5. Photocatalytic analysis

According to the theory of semiconductor photocatalysis, the strength of the photocatalyst is determined by its shape, band gap, surface area, particle size, crystalline nature, and quantity of hydroxyl ions on its surface (Pourahmad et al., 2010). According to the theory, when light is absorbed by a semiconductor, an electron and a hole are created on its surface. These electrons and holes will either participate in the process or recombine. If the charge carriers are given an external surface, they will move to the location where the semiconductor traps the electrons while the hydroxyl radicals trap the holes and produce OH^{\cdot} and HO_2^{\cdot} . Because there is more surface area available in ternary structures for the translocation of charge carriers, MB is effectively broken down by the generated hydroxyl ions. According to the UV–vis spectroscopy data, the produced heterostructure is active in both the UV–vis

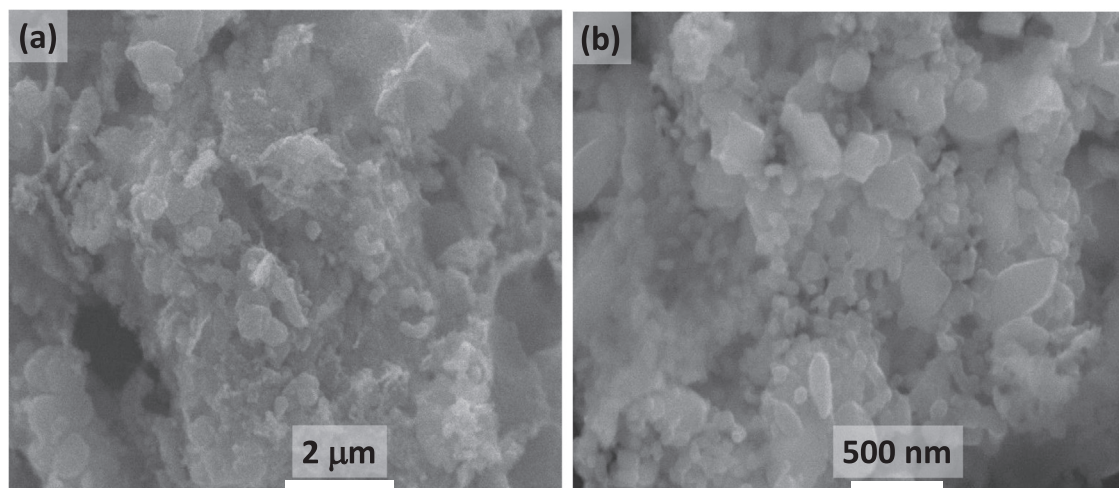


Fig. 4 FESEM images (a) and (b) of ZnO/CuO/Eu heterostructures at different magnifications.

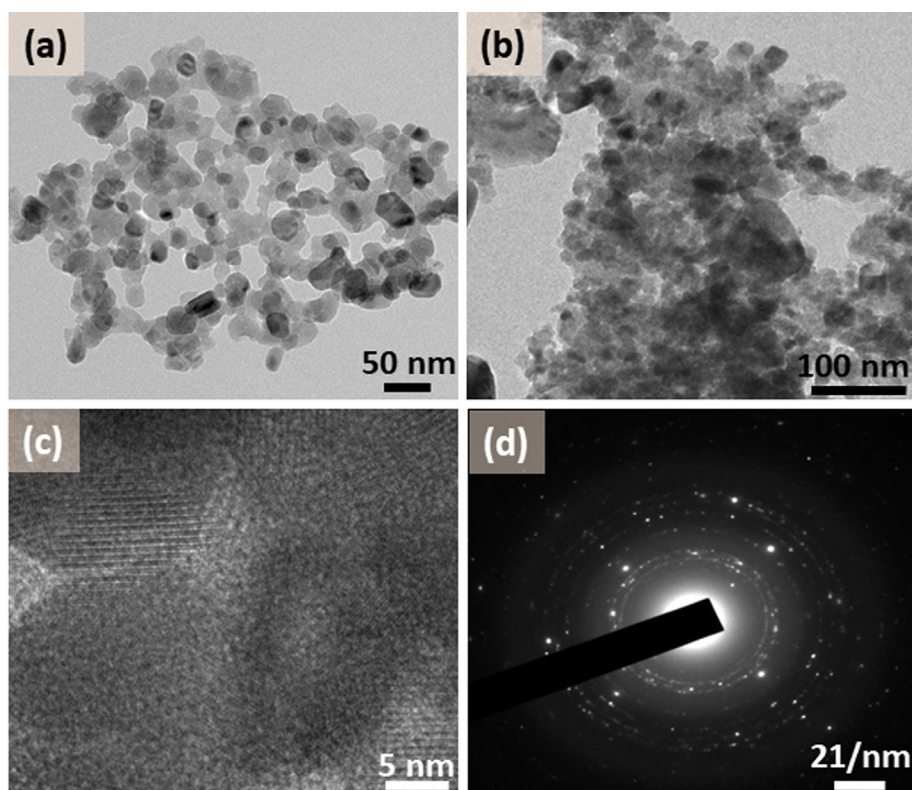


Fig. 5 TEM images of ZnO/CuO/Eu heterostructure with (a) low magnification, (b) high magnification showing particles, (c) HRTEM showing lattice fringes, and (d) electron diffraction image.

and the visible regions. Additionally, the computed band gap resulted in $E_g = 3.30$ eV.

MB and RB are used as the standard pollutant for photocatalytic degradation in the study, and the variation of absorption peak intensity recorded at 663 nm (λ_{\max} of MB and Effluent) and 568 nm (λ_{\max} of RB) is used to evaluate the photocatalytic performance of the heterostructure, i.e. ZnO/CuO/Eu. 100 mL of an aqueous solution with MB, RB concentrations of 5, 10, 15, and 20 ppm and while in the case of industrial effluent 5, 10, 15, and 20 mL are taken for the degradation experiments. There are different amounts of the as-prepared heterostructure are employed such as 5, 10, 15, and 20 mg of ZnO/CuO/Eu. The mixture is aerated for 40 min in the dark after being combined with mixed metal oxide. By routinely removing 3 mL of the aqueous mixture as a sample from the solution at intervals of 30 min and centrifuging it, it is possible to study the kinetics of the degradation. A similar procedure is followed by the reaction wherein the samples are exposed to UV irradiation or sunlight. The initial (C_i) and final (C_f) dye concentrations in the system are confirmed by the absorbance spectra obtained by using UV-vis spectroscopy, and the percentage of dye degradation is calculated by replacing the values obtained in Eq (1).

$$\% \text{ of degradation} = \frac{(C_i - C_f)}{C_i} \times 100 \quad (1)$$

A variety of parameters are studied for the optimization of the heterostructures such as light source, % of Eu doping, the dosage of catalyst & dyes, and, pH.

3.5.1. Effect of the light source

Since the as-prepared heterostructure is photolytically active in both the UV region and in the visible region as confirmed from the UV-vis spectra, the first set of studies is designed to confirm the light source that can yield the best performance of the as-prepared heterostructure. Hence, the photocatalytic degradation of MB and RB is carried out by employing the as-prepared catalyst, i.e. ZnO/CuO/3 wt% Eu heterostructures in three different environments, i.e. under sunlight, UV ray irradiation, and in the dark. In the case of the experiment carried out in the dark, the degradation of MB is found to be negligible i.e. $\sim 5\%$. However, in the case of exposure to visible light and UV, the degradation of MB obtained is 45% and 99%, respectively, which is significantly higher than the degradation obtained in the sample. In the case of degradation of RB, similar results are observed, a 37% and 93% degradation is obtained in case of exposure to visible light and UV, respectively, moreover, in the dark, the degradation activity against RB is the least. The graphical illustration is given in Fig. 6.

3.5.2. Influence of mole % of Eu doping

Three different samples of ZnO/CuO/Eu with varying wt.% of Eu (1 wt%, 3 wt%, and 5 wt%) are prepared. The photocatalytic efficiency of all the samples is tested. From the results obtained, it can be observed that the nanocomposite ZnO/CuO/1% wt. Eu starts with $\sim 20\%$ degradation of both the dyes tested i.e. MB and RB, however with the continuation of the reaction under sunlight the degradation proceeds to 8% and 76% degradation of the dyes MB and RB,

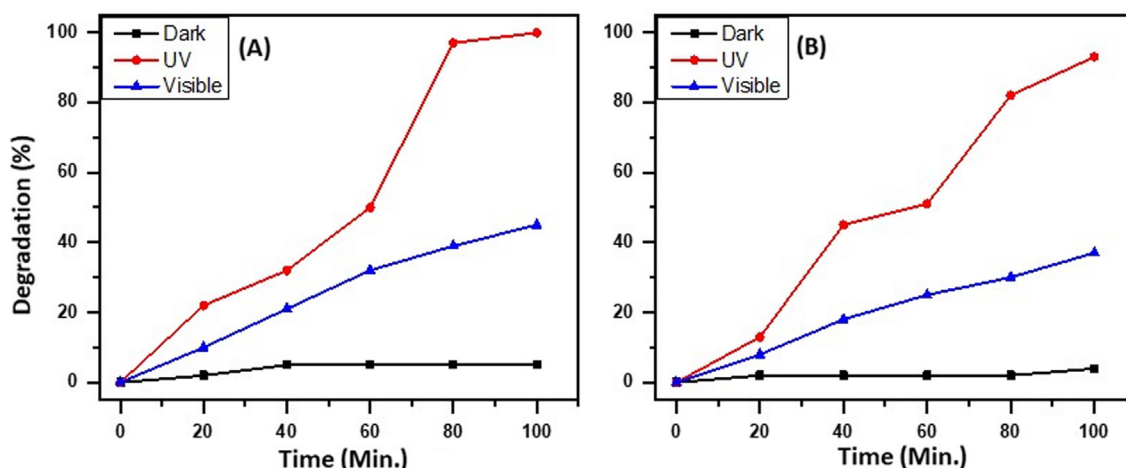


Fig. 6 Variation of the light source on the degradation of (A) MB and (B) RB.

respectively. With the catalyst with 3 wt% doping of Eu i.e. ZnO/CuO/3% wt. Eu exhibits a similar degradation pattern as that of 1% catalyst until 60 min of the reaction, however, there is a steep rise in the degradation of dyes until 80 min of the experiment and the % degradation of MB is more compared to RB, i.e. 97% and 82% within 80 min of reaction time. However, the degradation of MB proceeds towards complete degradation i.e. 100% within 100 min of reaction time. Moreover, with the ZnO/CuO/5% wt. Eu, a 78% and 70% photocatalytic degradation of MB and RB, respectively, is observed. Hence it is concluded that the 3 wt% of Eu is optimum for the best photocatalytic performance of the prepared nanoparticles. The results obtained for the photocatalytic degradation of MB and RB employing catalysts with varying percentages of Eu in the system are graphically illustrated in Fig. 7. Therefore, all further optimization studies for the degradation are carried out with catalyst ZnO/CuO/3% wt. Eu, i.e. 3 wt% Eu supported ZnO/CuO nanoparticles.

To further ascertain the role of Eu in the acceleration of the photocatalytic degradation of the dyes the photocatalytic activity of the as-prepared catalyst, that is, ZnO/CuO/3 wt% Eu is compared with the individual components of the catalyst, that is, ZnO and CuO under the similar experimental conditions. It is observed that the degradation of MB obtained is 20% and 62% while the degradation of RB obtained is 28% and 61%, respectively, which is much lower than the 99%, and 93% obtained from the use of the as-prepared catalyst,

indicating the synergistic effect of all the three components of the catalyst on the degradation of MB, and RB. The graphical illustration of the degradation of MB and RB using ZnO and CuO is given in Fig. 8.

3.5.3. Effect of amount of catalyst

In further continuation of the study after the confirmation of the optimum wt. % of Eu in the catalytic system and the source of light for the efficient photocatalytic performance of the as-prepared heterostructure, the optimum amount of catalyst for the degradation of MB and RB is evaluated by varying the catalyst in the range 5–20 mg with a constant dosage of MB and RB (6 ppm) under UV radiation. An 89% and 58% degradation of MB and RB is observed when 5 mg of photocatalyst is used. When the amount of catalyst is increased from 5 to 15 mg, and, an increase in the degradation of MB i.e. from 89% to 99% is observed, while in the case of RB the increase is significant i.e. from 58 to 93%. However, when the amount of catalyst is increased further to 20 mg, then a slight decrease in the degradation efficiency of the catalyst is observed in the case of MB i.e. from 99% to 97%, and, an increase in degradation is observed with regard to RB (97%). This reduction in the degradation efficiency with regard to MB may be due to accumulation and sedimentation of the catalyst particles at higher concentrations, which in turn causes the increase in light scattering, which results in a decrease in the light path inside the

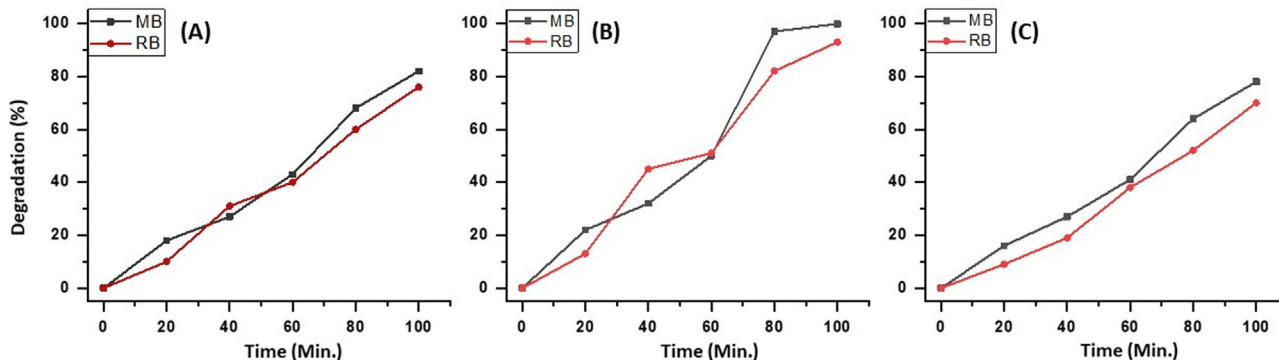


Fig. 7 The photo-degradation of industrial dyes MB and RB by employing X wt.% Eu supported ZnO/CuO nanoparticles (A) 1%, (B) 3%, and (C) 5%.

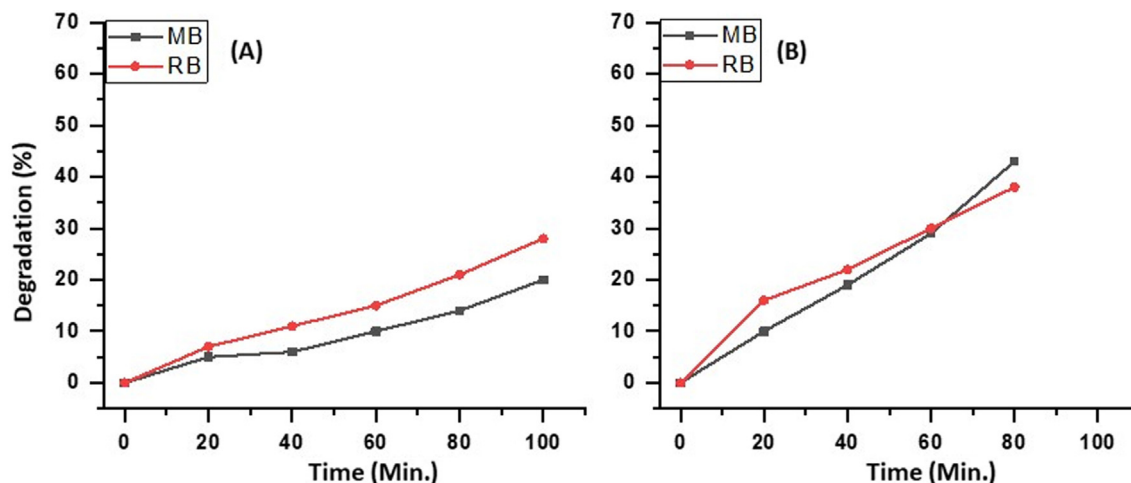


Fig. 8 Degradation of MB and, RB using (A) ZnO and (B) CuO.

solution; moreover, the higher concentration of the catalyst may also cause agglomeration of the photocatalyst, ensuing a decrease in the number of photocatalytic active sites (Ghaly et al., 2017; Pourahmad et al., 2010; Sakthivel et al., 2003). Hence, the optimum amount of photocatalyst for efficient degradation of MB is 15 mg and, in the case of RB is confirmed as 20 mg. The results obtained are graphically illustrated in Fig. 9.

3.5.4. Effect of concentration of dyes

Further, the efficiency of the as-synthesized heterostructure, i.e. ZnO/CuO/3 wt% Eu NPs, is evaluated for varying concentrations of MB and RB in the range of 3–12 ppm under UV irradiation with the amount of catalyst employed as 15 mg. From the results obtained, it is observed that the degradation of MB and RB decreased from 99 to 87% and 93 to 70%, respectively, when the concentration of dye is increased from 3 to 12 ppm. This may be attributed to the decreased absorption of light on the surface of the photocatalyst with an

increase in dye concentration, which leads to a reduction in the generation of hydroxyl radicals, playing an important role in the degradation of MB and RB present in the system. Therefore, it is essential to increase the suitable concentration of photocatalyst with increased dye concentration (Fig. 10).

3.5.5. Effect of pH

For decades, heterogeneous photochemical reactions on semiconductor surfaces have been investigated for their possible use as catalysts for the breakdown of organic contaminants and the splitting of water. Photogenerated electrons and holes can initiate reduction and oxidation reactions when they move to semiconductor surfaces. The high rate of photogenerated carrier recombination and the back-reaction of intermediate chemical species are two of the biggest issues. One possible way to boost the total photochemical reactivity has been the spatial separation of electrons and holes by internal fields or charged surfaces. For instance, a negatively charged (positively charged) surface domain will draw holes (electrons) and so

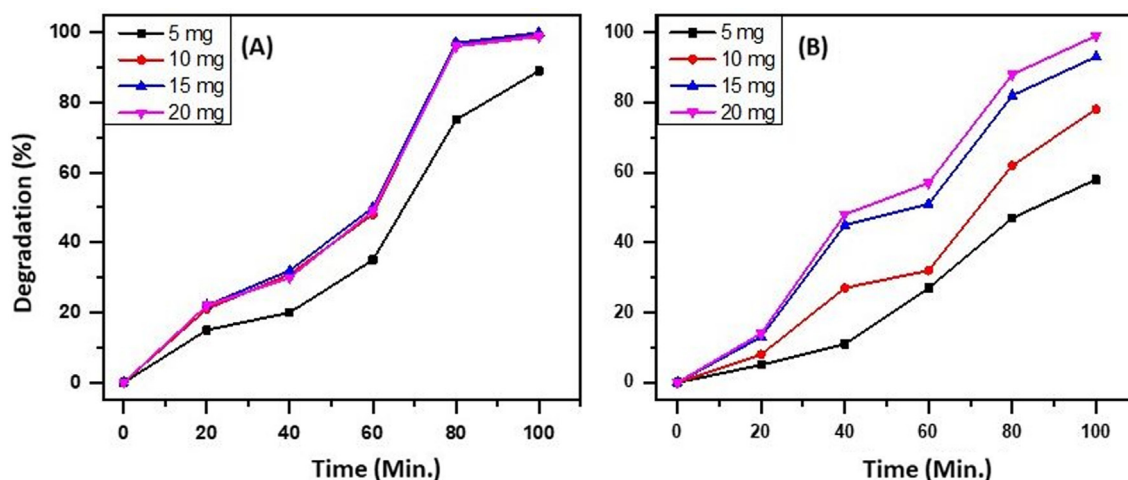


Fig. 9 Effect of variation of the amount of photocatalyst i.e. ZnO/CuO/3 wt% Eu NPs, on the degradation of (A) MB and (B) RB.

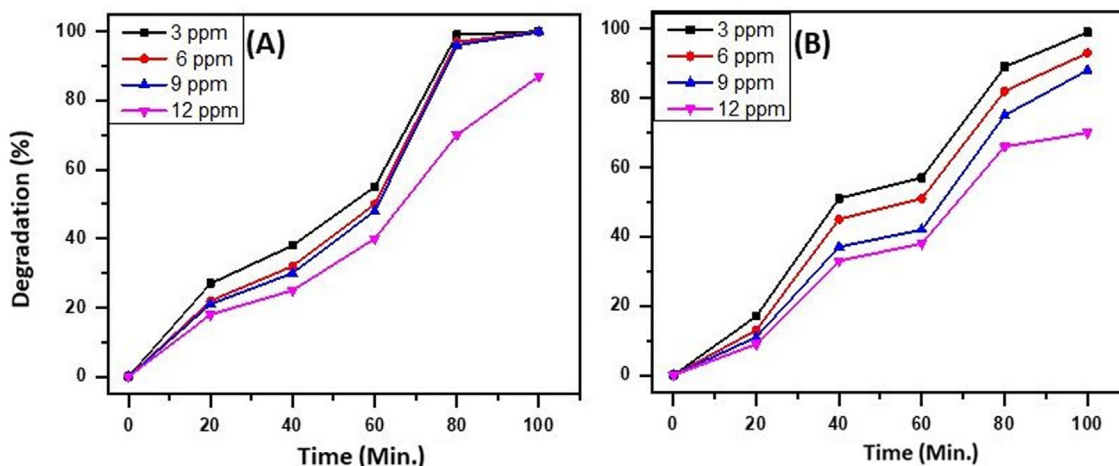


Fig. 10 Effect of variation of concentration of dye on the degradation efficiency of the ternary heterostructure i.e. ZnO/CuO/3 wt% Eu NPs, on (A) MB and (B) RB.

encourage the photoanodic (photocathodic) reaction. The overall reaction will be accelerated as long as the surface has both photoanodic and photocathodic domains. The slower half-reaction sets a maximum on the overall reaction rate since the two half-reactions must run at the same speed to maintain charge neutrality. The fastest reaction will slow down if a potential to speed up the slower reaction is applied, while the fastest reaction will speed up when a potential is applied to stop either of the two half-reactions from limiting the overall rate. By changing the pH, one can alter the potential of particles in a solution. The band bending in the semiconductor, the quantity of charge adsorbed on the surface, the surface potential, and the concentration of free charge carriers at the surface are all affected by the solution pH. The pH will have an impact on the total reaction rate since the photochemical reactivity is directly proportional to the quantities of accessible charge carriers. The results confirmed that the alteration of photocatalytic activity of ZnO/Eu/CuO is increased with pH from 4 to 10. The maximum photocatalytic activity of ZnO/Eu/CuO falls out at pH = 7. It may be attributed to the effect of Eu

and CuO nanoparticles on the recombination of generated electron-hole pairs. The Eu-doped ZnO/CuO nanoparticles (with a wider band gap) on the outer surface lead to the individuation of generated electron-hole pairs. Therefore, the increment of available surface improves the isolation of electron-hole pairs. Based on the results given in Figs. 11 and 12 B, it can be deduced that the photo-degradation of MB and RB at pH = 7 is higher than that of pH = 4 and pH = 10. As mentioned before the enhancement of the photocatalytic activity of the synthesized photocatalyst at pH = 7 may be due to the aggregation of charge on the outer surface of the photocatalyst. So, the variation of the pH can be affected the dispersibility of hybrids in the solution (Lingampalli et al., 2013; Manjunath et al., 2016).

3.6. Industrial effluent degradation study

With the excellent results obtained regarding the degradation of commonly used dyes such as MB and RB, the ternary heterostructure, i.e. ZnO/CuO/X wt.% Eu NPs, are put to test

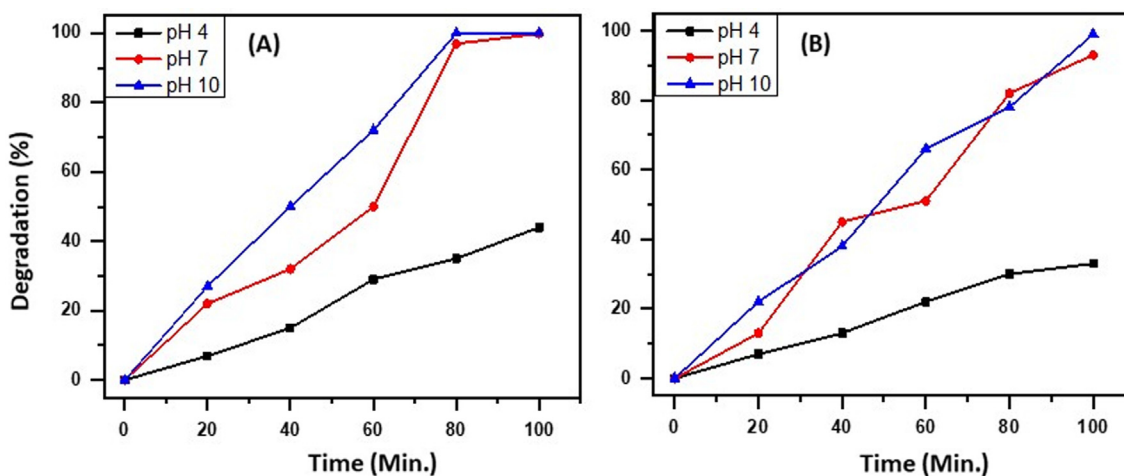


Fig. 11 Effect of variation of pH on the degradation efficiency of ZnO/Eu/CuO.

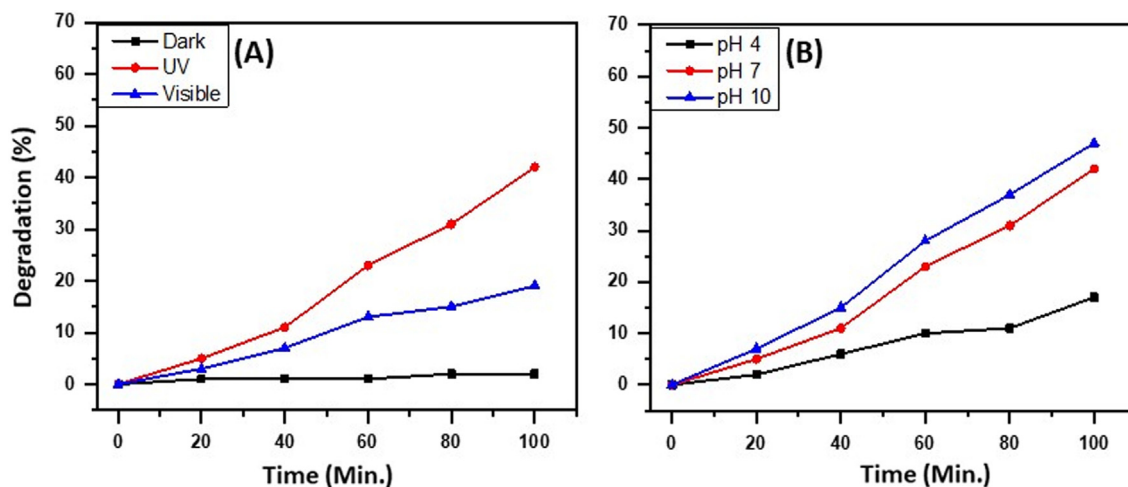


Fig. 12 Effect of (A) light sources and (B) pH on the degradation efficiency of the as-prepared ternary heterostructure, i.e. ZnO/CuO/X wt.% Eu NPs.

against the industrial effluent for their degradation efficiency in the real-time scenario. To begin with, the catalyst, i.e. ZnO/CuO/X wt.% Eu NPs, is tested for their activity in the presence of UV light, sunlight, and, in the dark for the degradation of industrial effluent. The results obtained are graphically illustrated in Fig. 12A. From the results obtained it can be observed that the degradation of the effluent is maximum when the solution is exposed to UV light with a 42% degradation of effluent is observed. The sunlight exposure yielded a 19% degradation of effluent and is negligible in the dark. The degradation of effluent is much lower than the degradation observed in the case of MB and RB, this can be due to the presence of other impurities which could block the active sites of the ternary heterostructure, unlike the pure MB and pure RB tested. Another study carried out is the effect of pH

on the degradation efficiency of the as-prepared ternary heterostructure, i.e. ZnO/CuO/X wt.% Eu NPs on the industrial effluent. The results are like the ones obtained about the degradation of MB and RB. In case, when the effluent solution is acidic or neutral the degradation efficiency of the as-prepared catalyst is low and when the pH is high i.e. 10, the degradation efficiency is the highest. The results are illustrated in Fig. 12B.

Regarding the amount of catalyst and the appropriate concentration of the effluent, it is observed that the ternary heterostructure behaves similar way as observed in the case of MB and RB. It is observed that as the amount of catalyst is increased the degradation of effluent is linear to the amount of catalyst. The variation in the amount of catalyst is carried out from 5 mg to 20 mg and the best degradation percentage

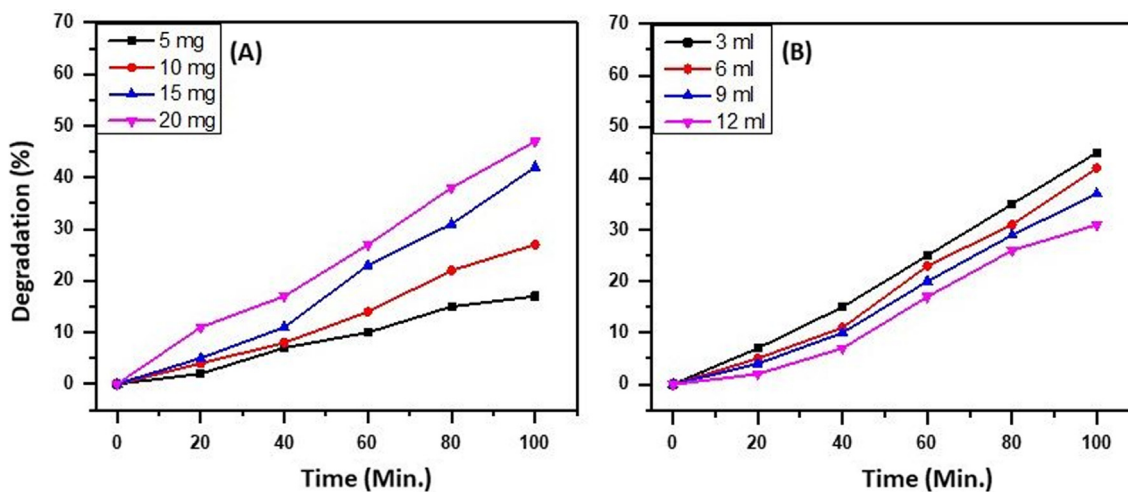
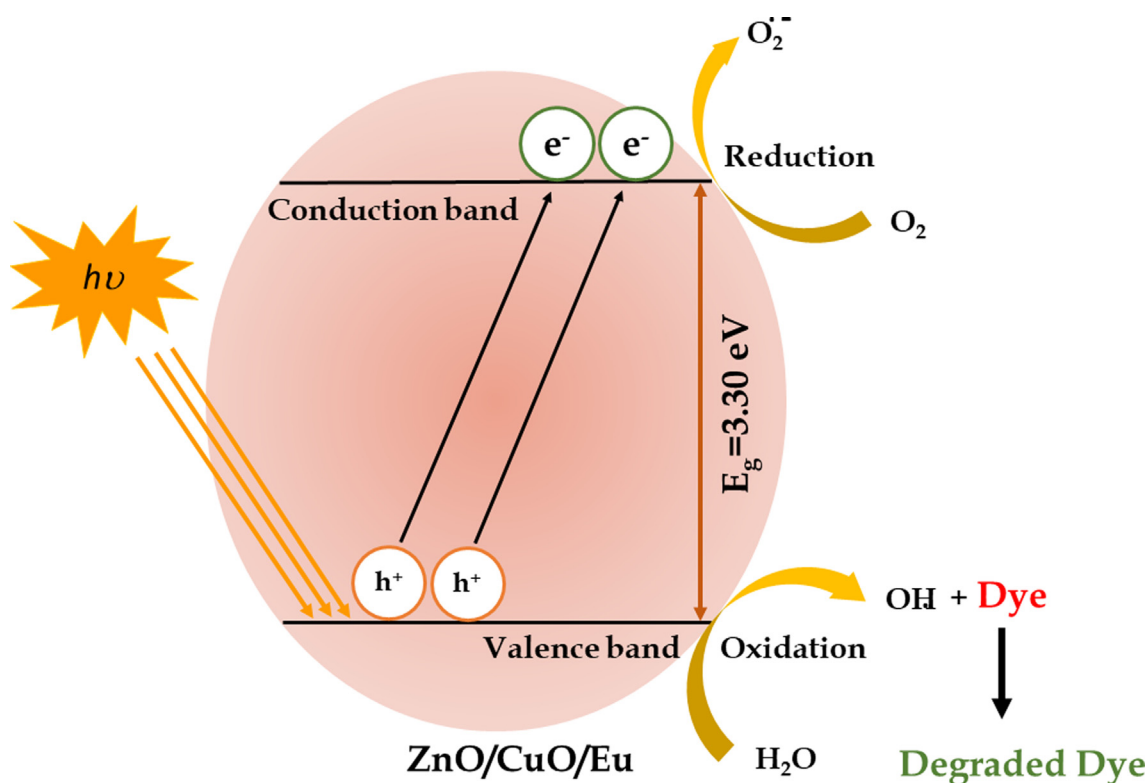


Fig. 13 Effect of (A) concentrations of catalyst and (B) effluent on the degradation efficiency of the as-prepared ternary heterostructure, i.e. ZnO/CuO/X wt.% Eu NPs.



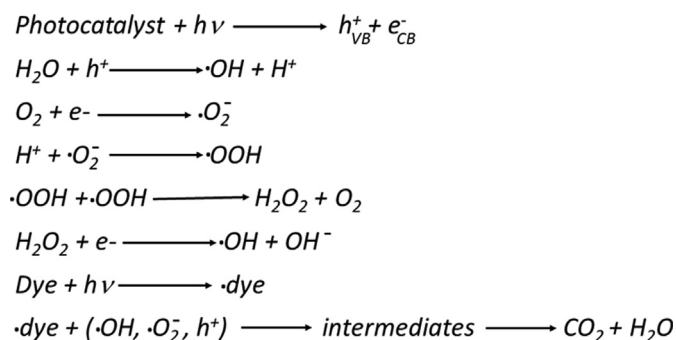
Scheme 1 A plausible mechanism for the degradation of dye.

is obtained when the effluent mixture is exposed to 20 mg of catalyst. The concentration of the effluent solution is also studied wherein the amount of effluent in the solution is varied from 3 mL to 12 mL and it is observed that as the concentration of effluent is increased, a decrease in the degradation percentage is observed. The results obtained are graphically illustrated in Fig. 13 A and B.

3.7. Photocatalytic mechanism

Based on the above experimental findings, a possible mechanism for the enhanced photocatalytic efficacy of ZnO/CuO/Eu photocatalyst upon visible light irradiation is proposed and schematically illustrated in Scheme 1. Under irradiation,

the ZnO/CuO/Eu photocatalyst can be readily excited, and electron-hole pairs are generated on its surface. Moreover, due to the presence of Eu doping in the photocatalyst, most probably sublevels beneath the conductive band are introduced and hence enhance the UV and visible light response (Kumar and Rao, 2017; Qi et al., 2017; Zheng et al., 2012). Hence, the excited electrons and holes could be efficiently separated, overturning the potential of charge carrier reunion; consequently, $\cdot\text{OH}$ active radicals are generated from the electrons in the CB over a two-electron oxidation path, which directly decomposes the organic pollutant, MB RB dyes or effluent. As a result, the photoinduced $\cdot\text{OH}$ and h^+ active radicals are responsible for the degradation, and the plausible mechanism is summed up as follows.



4. Conclusion

Herein, the feasibility of solution combustion synthesis (SCS) has been tested for the preparation of zinc oxide-based ternary heterostructure ZnO/CuO/Eu (1%, 3%, and 5% of Eu) photocatalyst. For this purpose, an environmental-friendly, waste cowpea skin extract was used as fuel, which has facilitated the formation of highly crystalline, ternary heterostructure particles, as a result of the highly exothermic conditions prevailing in SCS. The heterostructure photocatalyst demonstrated considerable enhancement towards the degradation of MB and RB under UV light irradiation, with ~99% removal of model compounds within 100 mins. However, in the case of the real sample i.e. industrial effluent, the photocatalytic activity was relatively low leading to a degradation of ~42% only, which could be due to the presence of a spectrum of dyes and the as-synthesized catalyst is not capable of degrading the entire spectrum of dyes and hence the degradation % is much less than the individual dyes tested. The results have revealed an optimum amount of photocatalyst and concentration of the dye is responsible for maximum degradation activity. Besides, several other parameters have also been investigated which contributed to the improvement of the photocatalytic performance of ZnO/CuO/Eu ternary heterostructure.

Declaration of Competing Interest

The authors declare that they have no known competing financial interests or personal relationships that could have appeared to influence the work reported in this paper.

Acknowledgment

The authors extend their appreciation to the Deputyship for Research & Innovation, Ministry of Education in Saudi Arabia for funding this research work through the project no. (IFKSURG-2-1688).

References

- Adil, S., Assal, M., Khan, M., Al-Warthan, A., Siddiqui, M.R.H., 2013. Nano Silver-Doped Manganese Oxide as Catalyst for Oxidation of Benzyl Alcohol and Its Derivatives: Synthesis, Characterisation, Thermal Study and Evaluation of Catalytic Properties. *Oxid. Commun.* 36, 778–791.
- Aruna, S.T., Mukasyan, A.S., 2008. Combustion synthesis and nanomaterials. *Curr. Opin. Solid State Mater. Sci.* 12, 44–50.
- Ataei, A., Mehrizad, A., Zare, K., 2021. Photocatalytic degradation of cefazoline antibiotic using zeolite-supported CdS/CaFe₂O₄ Z-scheme photocatalyst: Optimization and modeling of process by RSM and ANN. *J. Mol. Liq.* 328, 115476.
- Belver, C., Bedia, J., Gómez-Avilés, A., Peñas-Garzón, M., Rodriguez, J.J., 2019. Semiconductor photocatalysis for water purification. In: *Nanoscale materials in water purification*. Elsevier, 581–651.
- Bharagava, R.N., Chowdhary, P., 2019. Emerging and eco-friendly approaches for waste management. Springer.
- Chiu, Y.-H., Chang, T.-F.-M., Chen, C.-Y., Sone, M., Hsu, Y.-J., 2019. Mechanistic insights into photodegradation of organic dyes using heterostructure photocatalysts. *Catalysts* 9, 430.
- Dai, X., Rao, J., Bao, Z., Li, K., Feng, L., Song, D., Zhao, L., Li, W., Liu, X., Yi, S., 2022. Magnetic double-core@ shell MnO₂@ NiFe₂O₄ DE as a multifunctional scavenger for efficient removal of tetracycline, anionic and cationic dyes. *J. Colloid Interface Sci.* 628, 769–783.
- Dai, X., Zeng, H., Jin, C., Rao, J., Liu, X., Li, K., Zhang, Y., Yu, Y., Zhang, Y., 2021. 2D–3D graphene-coated diatomite as a support toward growing ZnO for advanced photocatalytic degradation of methylene blue. *RSC Adv.* 11, 38505–38514.
- Ghaly, H.A., El-Kalliny, A.S., Gad-Allah, T.A., Abd El-Sattar, N.E., Souaya, E.R., 2017. Stable plasmonic Ag/AgCl-polyaniline photoactive composite for degradation of organic contaminants under solar light. *RSC Adv.* 7, 12726–12736.
- Hannachi, Y., Hafidh, A., 2020. Preparation and characterization of novel bi-functionalized xerogel for removal of methylene blue and lead ions from aqueous solution in batch and fixed-bed modes: RSM optimization, kinetic and equilibrium studies. *J. Saudi Chem. Soc.* 24, 505–519.
- Hassaan, M.A., El Nemr, A., Madkour, F.F., 2017. Testing the advanced oxidation processes on the degradation of Direct Blue 86 dye in wastewater. *Egyptian J. Aquatic Res.* 43, 11–19.
- Hsiao, P.-H., Li, T.-C., Chen, C.-Y., 2019. ZnO/Cu₂O/Si nanowire arrays as ternary heterostructure-based photocatalysts with enhanced photodegradation performances. *Nanoscale Res. Lett.* 14, 1–8.
- Julien, C., Nazri, G., 1998. General overview of vibrational spectroscopy of layered transition-metal oxides. *MRS Online Proc. Library (OPL)* 548.
- Khan, S., Malik, A., 2014. Environmental and health effects of textile industry wastewater. In: *Environmental deterioration and human health*. Springer, 55–71.
- Kumar, A., Rout, L., Achary, L.S.K., Mohanty, S.K., Dash, P., 2017. A combustion synthesis route for magnetically separable graphene oxide–CuFe₂O₄–ZnO nanocomposites with enhanced solar light-mediated photocatalytic activity. *New J. Chem.* 41, 10568–10583.
- Kumar, S., Kumar, A., Kumar, A., Krishnan, V., 2020. Nanoscale zinc oxide based heterojunctions as visible light active photocatalysts for hydrogen energy and environmental remediation. *Cat. Rev.* 62, 346–405.
- Kumar, S.G., Rao, K.K., 2017. Comparison of modification strategies towards enhanced charge carrier separation and photocatalytic degradation activity of metal oxide semiconductors (TiO₂, WO₃ and ZnO). *Appl. Surf. Sci.* 391, 124–148.
- Lavand, A.B., Malghe, Y.S., 2015. Visible light photocatalytic degradation of 4-chlorophenol using C/ZnO/CdS nanocomposite. *J. Saudi Chem. Soc.* 19, 471–478.
- Lee, K.M., Lai, C.W., Ngai, K.S., Juan, J.C., 2016. Recent developments of zinc oxide based photocatalyst in water treatment technology: a review. *Water Res.* 88, 428–448.
- Lingampalli, S., Gautam, U.K., Rao, C., 2013. Highly efficient photocatalytic hydrogen generation by solution-processed ZnO/Pt/CdS, ZnO/Pt/Cd_{1-x}Zn_xS and ZnO/Pt/CdS_{1-x}Se_x hybrid nanostructures. *Energy Environ. Sci.* 6, 3589–3594.
- Lv, S.-W., Liu, J.-M., Wang, Z.-H., Ma, H., Li, C.-Y., Zhao, N., Wang, S., 2019. Recent advances on porous organic frameworks for the adsorptive removal of hazardous materials. *J. Environ. Sci.* 80, 169–185.
- Ma, L., Pei, X.-Y., Mo, D.-C., Heng, Y., Lyu, S.-S., Fu, Y.-X., 2019. Facile fabrication of NiO flakes and reduced graphene oxide (NiO/RGO) composite as anode material for lithium-ion batteries. *J. Mater. Sci.-Mater. El.* 30, 5874–5880.
- Malik, A., Grohmann, E., Akhtar, R., 2014. Environmental deterioration and human health. Springer 10, 978–994.
- Manjunath, K., Souza, V., Ramakrishnappa, T., Nagaraju, G., Scholten, J., Dupont, J., 2016. Heterojunction CuO-TiO₂ nanocomposite synthesis for significant photocatalytic hydrogen production. *Mater. Res. Express* 3, 115904.
- Mehrizad, A., Gharbani, P., 2014. Decontamination of 4-Chloro-2-Nitrophenol from Aqueous Solution by Graphene Adsorption: Equilibrium, Kinetic, and Thermodynamic Studies. *Pol. J. Environ. Stud.* 23.
- Mehrizad, A., Gharbani, P., 2017. Novel ZnS/carbon nanofiber photocatalyst for degradation of rhodamine 6G: kinetics tracking of operational parameters and development of a kinetics model. *Photochem. Photobiol.* 93, 1178–1186.

- Mohamed, W., Abu-Dief, A.M., 2018. Synthesis, characterization and photocatalysis enhancement of Eu₂O₃-ZnO mixed oxide nanoparticles. *J. Phys. Chem. Solids* 116, 375–385.
- Mosavi, S.A., Ghadi, A., Gharbani, P., Mehrizad, A., 2021. Photocatalytic removal of Methylene Blue using Ag@ CdSe/Zeoilite nanocomposite under visible light irradiation by Response Surface Methodology. *Mater. Chem. Phys.* 267, 124696.
- Natarajan, S., Bajaj, H.C., Tayade, R.J., 2018. Recent advances based on the synergetic effect of adsorption for removal of dyes from waste water using photocatalytic process. *J. Environ. Sci.* 65, 201–222.
- Navarro, P., Gabaldón, J.A., Gómez-López, V.M., 2017. Degradation of an azo dye by a fast and innovative pulsed light/H₂O₂ advanced oxidation process. *Dyes Pigm.* 136, 887–892.
- Padil, V.V.T., Černík, M., 2013. Green synthesis of copper oxide nanoparticles using gum karaya as a biotemplate and their antibacterial application. *Int. J. Nanomed.* 8, 889.
- Paiman, S.H., Rahman, M.A., Uchikoshi, T., Abdullah, N., Othman, M.H.D., Jaafar, J., Abas, K.H., Ismail, A.F., 2020. Functionalization effect of Fe-type MOF for methylene blue adsorption. *J. Saudi Chem. Soc.* 24, 896–905.
- Pandey, A., Kalal, S., Ameta, C., Ameta, R., Kumar, S., Punjabi, P.B., 2015. Synthesis, characterization and application of naïve and nano-sized titanium dioxide as a photocatalyst for degradation of methylene blue. *J. Saudi Chem. Soc.* 19, 528–536.
- Paździor, K., Bilińska, L., Ledakowicz, S., 2019. A review of the existing and emerging technologies in the combination of AOPs and biological processes in industrial textile wastewater treatment. *Chem. Eng. J.* 376, 120597.
- Pereira, L., Alves, M., 2012. Dyes—environmental impact and remediation, in: *Environmental protection strategies for sustainable development*. Springer, 111–162.
- Pirhashemi, M., Habibi-Yangjeh, A., Pouran, S.R., 2018. Review on the criteria anticipated for the fabrication of highly efficient ZnO-based visible-light-driven photocatalysts. *J. Ind. Eng. Chem.* 62, 1–25.
- Pourahmad, A., Sohrabnezhad, S., Kashefian, E., 2010. AgBr/nanoAlMCM-41 visible light photocatalyst for degradation of methylene blue dye. *Spectrochim. Acta, Part A* 77, 1108–1114.
- Qi, K., Cheng, B., Yu, J., Ho, W., 2017. Review on the improvement of the photocatalytic and antibacterial activities of ZnO. *J. Alloys Compd.* 727, 792–820.
- Qrajhdaghy, M., Mehrizad, A., Gharbani, P., Shahverdizadeh, G.H., 2022. Quaternary composite of CdS/g-C₃N₄/rGO/CMC as a susceptible visible-light photocatalyst for effective abatement of ciprofloxacin: Optimization and modeling of the process by RSM and ANN. *Process Saf. Environ. Prot.*
- Ranjith, K.S., Kumar, D.R., Ghoreishian, S.M., Huh, Y.S., Han, Y.-K., Kumar, R.R., 2020. A radially controlled ZnS interlayer on ultra-long ZnO-Gd₂S₃ core-shell nanorod arrays for promoting the visible photocatalytic degradation of antibiotics. *Nanoscale* 12, 14047–14060.
- Rovira, J., Domingo, J.L., 2019. Human health risks due to exposure to inorganic and organic chemicals from textiles: A review. *Environ. Res.* 168, 62–69.
- Saif, S., Tahir, A., Asim, T., Chen, Y., Adil, S.F., 2019. Polymeric nanocomposites of iron-oxide nanoparticles (IONPs) synthesized using Terminalia chebula leaf extract for enhanced adsorption of arsenic (V) from water. *Colloids Interfaces* 3, 17.
- Sakthivel, S., Neppolian, B., Shankar, M., Arabindoo, B., Palani-chamy, M., Murugesan, V., 2003. Solar photocatalytic degradation of azo dye: comparison of photocatalytic efficiency of ZnO and TiO₂. *Sol. Energy Mater. Sol. Cells* 77, 65–82.
- Shaik, M.R., Adil, S.F., Kuniyil, M., Sharif, M., Alwarthan, A., Siddiqui, M.R.H., Ali, M.I., Tahir, M.N., Khan, M., 2020. Facile Sonochemical Preparation of Au-ZrO₂ Nanocatalyst for the Catalytic Reduction of 4-Nitrophenol. *Appl. Sci.* 10, 503.
- Shubha, J.P., Adil, S.F., Khan, M., Hatshan, M.R., Khan, A., 2021. Facile fabrication of a ZnO/Eu₂O₃/NiO-Based ternary heterostructure nanophotocatalyst and its application for the degradation of methylene blue. *ACS Omega* 6, 3866–3874.
- Siddique, F., Gonzalez-Cortes, S., Mirzaei, A., Xiao, T., Rafiq, M., Zhang, X., 2022. Solution combustion synthesis: the relevant metrics for producing advanced and nanostructured photocatalysts. *Nanoscale* 14, 11806–11868.
- Tabatabaei, S., Dastmalchi, S., Mehrizad, A., Gharbani, P., 2011. Enhancement of 4-nitrophenol ozonation in water by nano ZnO catalyst.
- Varma, A., Mukasyan, A.S., Rogachev, A.S., Manukyan, K.V., 2016. Solution combustion synthesis of nanoscale materials. *Chem. Rev.* 116, 14493–14586.
- Wang, M., Tan, G., Ren, H., Xia, A., Liu, Y., 2019. Direct double Z-scheme O_g-C₃N₄/Zn₂SnO₄/ZnO ternary heterojunction photocatalyst with enhanced visible photocatalytic activity. *Appl. Surf. Sci.* 492, 690–702.
- Wang, Y., Dai, X., Zhou, Q., Li, K., Feng, L., Liao, W., Yu, Y., Yu, H., Zong, X., Lu, G., 2022. Insights into the role of metal cation substitution on the anionic dye removal performance of CoAl-LDH. *Colloids Surf., A* 636, 128139.
- Wei, P., Yu, X., Li, Y., 2019. Preparation of Fe₃O₄/ZnO/ZnS Composites with Enhanced Photoperformance Under Solar Irradiation. *J. Electron. Mater.* 48, 4877–4885.
- Wen, W., Wu, J.-M., 2014. Nanomaterials via solution combustion synthesis: a step nearer to controllability. *RSC Adv.* 4, 58090–58100.
- Wetchakun, K., Wetchakun, N., Sakulsermsuk, S., 2019. An overview of solar/visible light-driven heterogeneous photocatalysis for water purification: TiO₂-and ZnO-based photocatalysts used in suspension photoreactors. *J. Ind. Eng. Chem.* 71, 19–49.
- Wu, L., Zhang, X., Thorpe, J.A., Li, L., Si, Y., 2020. Mussel-inspired polydopamine functionalized recyclable coconut shell derived carbon nanocomposites for efficient adsorption of methylene blue. *J. Saudi Chem. Soc.* 24, 642–649.
- Xu, C., Manukyan, K.V., Adams, R.A., Pol, V.G., Chen, P., Varma, A., 2019. One-step solution combustion synthesis of CuO/Cu₂O/C anode for long cycle life Li-ion batteries. *Carbon* 142, 51–59.
- Yu, X., Wei, P., Li, Y., 2019. Enhanced sunlight photocatalytic performance of ZnO/ZnS binary heterostructure sheets. *Mater. Lett.* 240, 284–286.
- Zak, A.K., Razali, R., Abd Majid, W.H., Darroudi, M., 2011. Synthesis and characterization of a narrow size distribution of zinc oxide nanoparticles. *Int. J. Nanomed.* 6, 1399–1403.
- Zeelani, G.G., Ashrafi, A., Dhakad, A., Gupta, G., Pal, S.L., 2016. Catalytic Oxidative desulfurization of liquid fuels: A review.
- Zheng, Y., Lin, J., Wang, Q., 2012. Emissions and photocatalytic selectivity of SrWO₄: Ln³⁺ (Eu³⁺, Tb³⁺, Sm³⁺ and Dy³⁺) prepared by a supersonic microwave co-assistance method. *Photochem. Photobiol. Sci.* 11, 1567–1574.